Physics and Imaging in Radiation Oncology 12 (2019) 10–16

Contents lists available at ScienceDirect

Physics and Imaging in Radiation Oncology

journal homepage: www.elsevier.com/locate/phro

An ultrasound based platform for image-guided radiotherapy in canine bladder cancer patients

Justin T. Sick[a], Nicholas J. Rancilio[b], Caroline V. Fulkerson[b], Jeannie M. Plantenga[a,b,c], Deborah W. Knapp[b,c], Keith M. Stantz[a,d,*]

[a] School of Health Sciences, Purdue University, 550 Stadium Mall Drive, West Lafayette, IN 47907, USA
[b] Department of Veterinary Clinical Sciences, Purdue University College of Veterinary Medicine, 625 Harrison Street, West Lafayette, IN 47907, USA
[c] Purdue University Center for Cancer Research, Purdue University, 201 S University St, West Lafayette, IN 47906, USA
[d] Department of Radiology, Indiana University School of Medicine, 550 University Blvd, Indianapolis, IN, 46202, USA

ARTICLE INFO

Keywords:
Ultrasound guided radiation therapy
Bladder cancer
Multimodal registration
Agar-based tissue equivalent phantom
3D printing

ABSTRACT

Background and purpose: Ultrasound (US) is a non-invasive, non-radiographic imaging technique with high spatial and temporal resolution that can be used for localizing soft-tissue structures and tumors in real-time during radiotherapy (RT) (inter- and intra-fraction). A comprehensive approach incorporating an in-house 3D-US system within RT is presented. This system is easier to adopt into existing treatment protocols than current US based systems, with the aim of providing millimeter intra-fraction alignment errors and sensitivity to track intra-fraction bladder movement.

Materials and methods: An in-house integrated US manipulator and platform was designed to relate the computed tomographic (CT) scanner, 3D-US and linear accelerator coordinate systems. An agar-based phantom with measured speed of sound and densities consistent with tissues surrounding the bladder was rotated (0–45°) and translated (up to 55 mm) relative to the US and CT coordinate systems to validate this device. After acquiring and integrating CT and US images into the treatment planning system, US-to-US and US-to-CT images were co-registered to re-align the phantom relative to the linear accelerator.

Results: Statistical errors from US-to-US registrations for various patient orientations ranged from 0.1 to 1.7 mm for x, y, and z translation components, and 0.0–1.1° for rotational components. Statistical errors from US-to-CT registrations were 0.3–1.2 mm for the x, y and z translational components and 0.1–2.5° for the rotational components.

Conclusions: An ultrasound-based platform was designed, constructed and tested on a CT/US tissue-equivalent phantom to track bladder displacement with a statistical uncertainty to correct and track inter- and intra-fractional displacements of the bladder during radiation treatments.

1. Introduction

Spontaneous invasive urothelial carcinoma (InvUC), also referred to as invasive transitional cell carcinoma, is the most common cancer of the canine urinary system and is only partially responsive to surgical resection or treatment with systemic chemotherapy [1]. Pilot clinical studies and case reports show radiation therapy (RT) is well tolerated, with no significant complications and improved urinary clinical symptoms being reported [2,3]. For optimal RT, and in order to minimize toxicity, changes in bladder volume, position and shape, must be accounted for, not just from day to day (inter-fractional changes) but for the duration of treatment (intra-fractional changes). To account for these changes, treatment margins are increased exposing the surrounding normal tissue. Hence, RT remains underutilized in InvUC because of the inability to accurately target the urinary bladder during treatment [4]. As with canine patients, human patients with an invasive nonresectable form of bladder cancer or requiring bladder conserving procedures would also benefit from RT, in particular intensity-modulated RT (IMRT), if the inter- and intra-fractional target motion could be adequately monitored and managed [5]. Thus, the technical development of image-guided devices and techniques to visualize a patient's internal anatomy during treatment has become an important and area of active research [6–8], although, no universally accepted commercial imaging system currently exists to accurately target the urinary bladder

* Corresponding author at: 550 Stadium Mall Drive, West Lafayette, IN, 47907, USA.
E-mail address: kstantz@purdue.edu (K.M. Stantz).

https://doi.org/10.1016/j.phro.2019.10.003
Received 14 May 2019; Received in revised form 7 October 2019; Accepted 9 October 2019

in real time during treatment.

Current image-guided radiation therapy (IGRT) systems make use of a variety of different radiographic and non-radiographic modalities to monitor and reduce uncertainties associated with internal organ location and motion. The most common image guidance systems use radiographic, fluoroscopic, or cone beam computed tomography (CBCT). These systems not only introduce an additional, non-negligible dose to the patient [9], but align the patient based on their skeletal features, not necessarily the target volume or bladder. MRI provides superior onboard 3D imaging of soft tissue, but remains in the developmental stage, is expensive, and excludes patients with metal implants and pacemakers. Ultrasound (US) imaging provides a cost-effective non-invasive alternative for treatment setup and real time (3D) target tracking without introducing additional dose to the patient.

To date, a number of ultrasound (US) external beam radiation therapy (EBRT) guidance systems have been developed [10–12], each with its advantages and disadvantages. Some of the deficiencies include the dependency of the operator, where the applied pressure can distort patient anatomy; or the introduction of expensive robotics and positioning systems. In this paper, a low-cost hands-free US-based platform has been designed, fabricated and integrated into the radiation treatment protocol. To evaluate the feasibility of this device, a tissue-equivalent agar-based bladder phantom was constructed and used to evaluate couch realignment uncertainties based on rigid-body image registration of 3D US and computed tomographic (CT) images. Thus, the aims of this study are to, first, demonstrate that this device can achieve phantom alignment errors within a few millimeters, consistent with existing on-board radiographic imaging systems, and second, to demonstrate that 3D US can provide enough sensitivity to track bladder movement, consistent with bladder filling or emptying.

2. Materials and methods

2.1. Construction of 3D US platform

The objective of the US-based platform design was to provide a common coordinate system between the treatment planning CT and the linear accelerator (linac), where 3D ultrasonic images would be used to determine the translation and rotation matrix between these two coordinate systems. The resulting design of the US-based platform implements an adaptable manipulator to provide discrete reproducible (or calibrated) positions with errors less than the positional uncertainties of the linac couch, with minimal cost and complexity. The key aspects of the platform are to: (1) place and locate the transducer array (TA) with submillimeter precision; (2) change the angle of the TA to provide a means to optimize image fidelity; (3) assemble and disassemble quickly and easily around the patient on the CT and linac couches; and (4) use materials that will not affect RT dosimetry. Acrylic was used due to its low cost, low atomic mass and density, and ease with which it can be manufactured. The parts that could not be manufactured were 3D printed. The final design can be seen in Fig. 1.

The frame was designed to be assembled around the patient after the patient was positioned using laser alignment. A set of “slots” or discrete locations for the translating stage to rest in were included, where each slot was placed 5 cm apart laterally from the center, and a discrete set of angles in 15° increments, in order to vary the position the transducer array (TA) obliquely. The extension of the radial arm and the longitudinal shifts were done with a 1 mm threaded rod which gives us increments as fine as 10 μm. As a result, a high precision for the transducer-patient interface was available and if a 3D array was to be used, small slice thicknesses could be achieved. When a patient was positioned on the linac couch, any deviations in the platform settings (from simulation) were used as inputs to the software interface to realign the patient.

A critical step in the US-platform design was a clamp or mold to hold and position the TA with high reproducibility, thus defining the central axis of the TA within the platform’s geometry that was related to the coordinate systems of the linear accelerator and CT couch. A CT safe placeholder of the TAs, which was modeled from 3D infrared surface scans, were 3D printed using filament-based thermoplastics method. With these surface renderings, clamps were designed to form-fit each transducer array. Individual clamps were designed to be interchangeable with the platform.

To evaluate the uncertainty in patient realignment, the arm of the platform that holds the TA was positioned at the treatment room isocenter, then the TA was rotated through each discrete angle and the RT couch was repositioned for the central ray normal to the TA surface to align with isocenter. The average and standard deviation (SD) were calculated through repeating this process.

2.2. Developing a urological phantom of the bladder

An agar-based tissue-equivalent phantom was constructed to recreate US and CT density consistent with bladder cancer patients and used to integrate the US-based platform into the treatment planning protocol. The acoustic and x-ray attenuation properties of this phantom were designed to be representative of the urinary bladder and surrounding tissues. The anatomical features and dimensions were obtained from CT and US scans of canine patients within the Purdue Veterinary Teaching Hospital. This phantom was molded in a $12 \times 12 \times 12\,cm^3$ acrylic container, with a 3 mm layer of skin, 1 cm layer of fat, 1 cm layer of muscle, and 25 mL ellipsoid (balloon) of 5% NaCl saline (urine) embedded within a 7 cm layer of soft tissue. The CT and 3D US images of the bladder phantom are displayed in Fig. 2. The phantom was a mixture of agar, glycerin and physiological saline, where the proportion of each ingredient was chosen to produce CT density and speed-of-sound consistent with skin, muscle, fat and bladder.

Methods were developed to produce and ensure a uniform set of acoustic (speed-of-sound) and CT (density) properties within each tissue type over the duration of the study. Each tissue was designed with a speed-of-sound based on mixtures of distilled water, agar (0–2%), and glycerin (0–100%) using a linear model:

$$C_{g/w} = g * 1920\left[\frac{m}{s}\right] + w * 1494\left[\frac{m}{s}\right](\text{at } 25\,^{\circ}\text{C}) \quad (1)$$

where g is the fraction by volume of glycerin within distilled water ($w = 1 - g$). The 2% agar resulted in a 10 m/s increase. Based on values found in the literature, skin, muscle, and fat consisted of 50, 25, and 0% glycerin and 2% agar, while urine consisted of 5% saline (NaCl) (Table 1). The speed of sound for each tissue component was measured independently during fabrication based on the calibration curves using photoacoustic methods. Tissue density was measured from CT scans, where the average HU value was converted to a density based on the calibration curve obtained from scans of a QA CT phantom (Gammex 464 ACR CT Phantom).

2.3. Image registration

B-mode ultrasonography of all phantoms was performed with a dedicated ultrasonography machine (Philips iU22 SonoCT system, Philips Ultrasound, Bothell, WA). A broadband volume curved array transducer (6–2 MHz) and/or a broadband volume linear array transducer (13–5 MHz) were utilized. The depth, focal spot and window level were adjusted to optimize image quality, resulting in a 512×510 matrix with a $0.42 \times 0.30 \times 0.60$ mm voxel size. The probes were positioned in a transverse plane for all imaging studies. All phantoms were scanned using a 64-slice helical CT scanner (GE Lightspeed 64 Slice CT Milwaukee, WI, USA) using the following parameters: kVp of 120, mA of 300–500, slice thickness of 2.5 mm, pitch of 1.0, variable scan field of view, 512×512 matrix, rotation time of 1 s. Resulting in a $0.54 \times 0.54 \times 2.5$ mm voxel size.

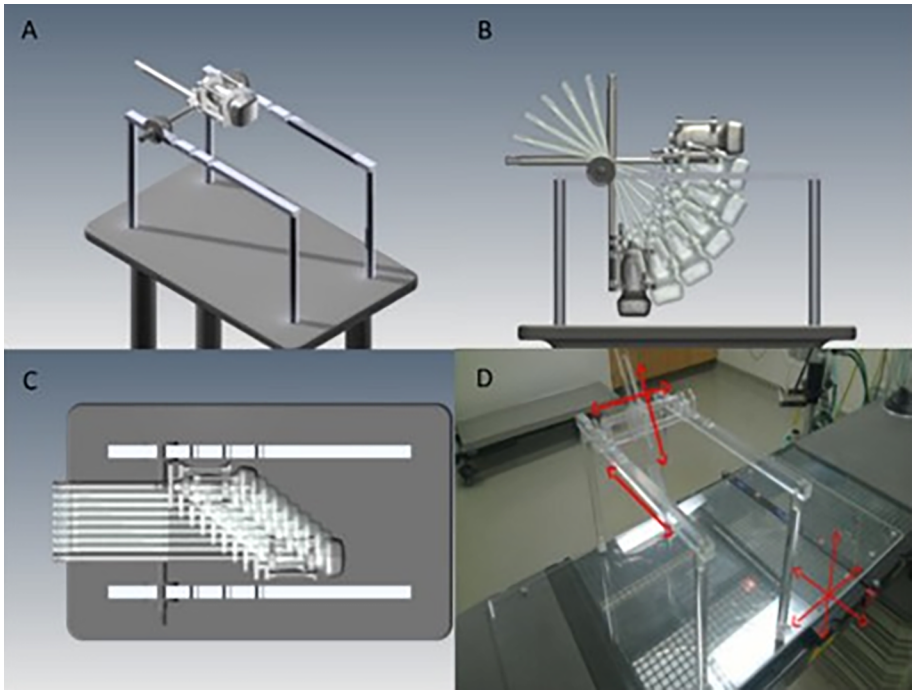

Fig. 1. Platform Design. (A) Overview of the platform design, (B) Different possible discrete angles of the transducer, (C) Longitudinal and lateral range, and (D) different coordinate systems of the US guidance platform and the RT treatment bed.

All registrations were made using Eclipse™ treatment planning system (Platform Version 11.0; Varian Medical Systems Inc., Palo Alto, CA, USA) in order to avoid introducing additional software to the treatment planning process. In order for Eclipse™ to recognize the US images, a MATLAB™ (R2019a, MathWorks, Inc., Natick, MA, USA) script was developed to create DICOM files for the 3D-US volumes by modifying the DICOM headers and slice image data from a copy of the treatment CT scan. Unlike CT where each slice stands on its own, the US volumes are exported from the unit as one 3D matrix. A script was written to separate each slice from the exported volume, assign new metadata with the correct positional (couch and platform) and voxel information (from US) and write new DICOM images. The files could then be imported into Eclipse™ using the DICOM media file import filter as if they were CT scans.

Critical to this protocol was the ability to accurately and precisely co-register the US volume (linac) to the simulation CT volume, and the US volume to the initial or baseline US volume once patient alignment to the simulation CT volume has been performed. To measure these parameters, the bladder phantom was translated and rotated relative to the US TA. The experimental setup for these tests is shown in Fig. S1. For each measurement, the phantom was rotated (using a rotating platform) over a 0–45° range – at angles rotated 5, 15, 30 and 45° around the vertical axis – and translated within a 7 cm range, after which a CT and US scan was acquired. This procedure was repeated after inserting a 4° wedge to change the patient pitch.

Table 1
Physical Properties of the Tissue-Equivalent Bladder Phantom.

	Recipe		Measured		
	Glycerine (%)	Agar (%)	CT Number (HU)	Density (g/cm^3)	Speed of Sound (mm/μs)
Water	0	0	−1.2 ± 2.6	0.99	1.49
Skin	50	2	107.3 ± 3.5	1.10	1.70
Fat	0	2	2.6 ± 2.6	0.99	1.49
Muscle	25	2	69.6 ± 3.9	1.06	1.59
Urine	0	0	41.5 ± 0.8	1.03	1.55

Each subsequent scan (e.g. treatment) was co-registered to the original scan (e.g. simulation). The registration matrices composed of the x, y and z translation and rotational components were recorded. For the US scans, the TA was held in a clamp above the phantom and the experiment was repeated three times for each set of rotation angles (N = 3). The US-to-US and US-to-CT co-registrations were compared to the CT-to-CT co-registration.

Prior to co-registration, no manual movements or changes were made to the image volumes, in other words, an automatic registration was attempted. The details powering the Eclipse™ automatic

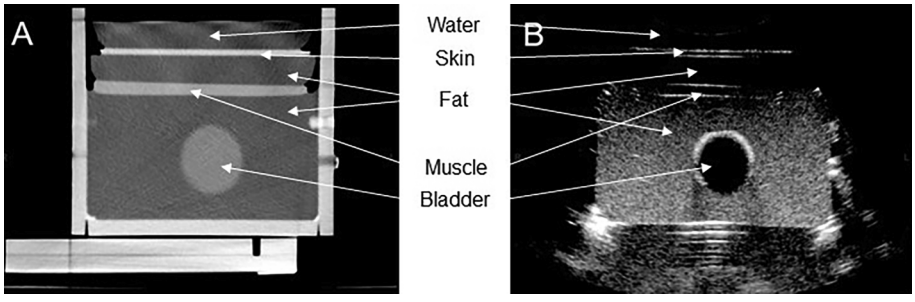

Fig. 2. Images of the urological phantom. (A) CT slice of phantom, (B) corresponding US slice.

registration are proprietary, but the underlying merit function was based on mutual information. If by visual inspection the automatic registration failed, then a rough manual match was applied. If the automatic registration still failed, then the field of view was modified to only include the phantom, then the bladder, skin and muscle and finally just the bladder. Lastly, image intensity thresholds were adjusted if all else failed. All US-to-US and CT-to-CT registrations could be automatically registered whereas the US-to-CT registrations were done manually.

The US-to-US and US-to-CT registrations were used to determine the accuracy and precision, where CT-to-CT registrations was used as our control group. Accuracy was measured by calculating the average difference in translational and rotational components of the transformation matrix between two registered volumes. Precision was determined by calculating the standard deviation (SD) of the transformation matrix components. Each US volume was registered to the phantom in the flat position for US and CT. The US-to-CT transformation matrices were subtracted from the average US-to-CT initial offset transformation matrix to correct for different initial coordinate systems.

3. Results

3.1. Construction of 3D-US platform

The errors between the geometry of the platform and the true couch readings were 0.2 ± 0.8 mm (lateral), 0.0 ± 1.0 mm (vertical), and 0.1 ± 0.7 mm (longitudinal). The overall uncertainty was measured to be 0.2 ± 1.5 mm.

3.2. Development of bladder phantom

The density and speed of sound for each tissue type within the bladder phantom were determined based on the measured calibration curves shown in Fig. S2. The resulting densities for water, skin, fat, muscle and urine within the canine bladder phantom were 0.99, 1.10, 0.99, 1.06, and 1.03 g/cm^3, respectively. For the same tissue types, the measured values for the speed of sound were 1.49, 1.70, 1.49, 1.59 and 1.55 mm/μs (Table 1).

3.3. Image registration

CT-to-CT registrations were found to automatically converge without the need for user input, while US-to-US and US-to-CT registrations required some initial manual alignment, specifically for larger rotation angles, as summarized in Table 2 (see Fig. 3 and Fig. S3). When compared to CT-to-CT registrations (controls), US-to-CT translational offsets along the x, y, and z-axes were kept below, on average, 2.0 mm if phantom rotational re-positioning was less than 5 degrees (wedge and 5 degrees data): average error in x (−0.4 ± 0.8 mm), y (0.1 ± 0.6 mm) and z (−1.9 ± 0.9 mm). Larger rotations increased this error to 2.0 mm and higher. Overall, the statistical errors from US-to-CT registrations were larger than those from US-to-US registrations. For the latter, errors were small, an average 0.4, 0.2, 0.8 mm along the x, y and z translational components, respectively, and 0.2°, 0.4° and 0.2° for the x, y and z rotational axis'. For the former, the statistical errors increased, with an average value of 0.7, 0.6 and 0.8 mm along the x, y and z translational components, respectively, and 1.2°, 0.9° and 0.6° for the x, y and z rotational axis'.

Table 2
Level of user intervention required to achieve a quality registration.

	CT-to-CT	US-to-US	US-to-CT
Wedge Only	Automatic	Automatic	Manual
5	Automatic	Automatic	Manual
15	Automatic	Initial manual alignment	Manual
45	Automatic	Initial manual alignment	Manual

*Automatic, The automatic registration successfully registered the datasets every time.
**Initial manual alignment, the user had to only roughly shift and rotate the target dataset before applying the automatic registration. Once a manual rough alignment was done, the automatic registration would be successful.
***Manual, the user had to apply multiple techniques to register the datasets. The automatic registration was never successful.

4. Discussion

The motivation for this study was to design, construct and integrate a 3D US-based platform that would allow radiation therapy to be incorporated into the treatment protocol of canine patients with localized bladder cancer. Due to inter- and intra-fractional positional changes of the bladder, large margins (1.5–2.0 cm) must be applied to avoid geographic miss in the absence of image guidance. The resulting increased normal tissue volumes in the irradiated field may increase the probability of normal tissue complications. To track bladder displacement and rotation, volumetric image registration based on soft tissue contrast was used to track these movements. An US-based platform was constructed and calibrated to provide a common coordinate system between the CT (treatment plan), linear accelerator (treatment delivery), and 3D ultrasound, thereby reducing the dose to the patient's normal tissues and providing a hands-free low-cost solution for inter-fraction target realignment and intra-fraction real-time motion assessment. The US-based platform was calibrated with a 1.5 mm (SD) uncertainty, consistent with the positional accuracy of the linear accelerator couch positioning system [9,13–15]. This device was tested using an US/CT tissue equivalent phantom with physical and geometric properties consistent with canine patients (Table 3) and used to evaluate realignment uncertainties. CT-to-US registration (inter-fraction) identified the bladder location with < 2 mm uncertainty, if initial patient laser alignment was within 5° rotational angles. Similarly, baseline-US to US registration was able to locate the relative bladder location within 2 mm, under various patient orientations. These positional uncertainties are in-line with existing radiological systems and with sufficient fidelity to track intra-fractional changes.

To date, there have not been any studies investigating the use of 3D US to improve bladder cancer radiation treatment in canine patients. There is also an important need for relevant animal models of invasive bladder cancer to test new therapies prior to clinical trials in humans [16]. InvUC in the canine patient offers many benefits that translate to the human disease, including similar biological behavior, histopathological appearance, drug metabolism, spontaneous occurrence, and therapeutic treatments [1]. For the latter, the challenges in applying radiation therapy in canine patients are the same as those in human patients, where changes in bladder position, volume and shape can result in inadequate dose to the bladder and increased dose to the surrounding normal tissues. Adaptive image guided techniques are urgently needed to increase the safety and effectiveness of radiotherapy for bladder cancer. Thus, the performance of US-based platform and phantom will be compared to similar systems applied to human patients.

Bladder movement and changes in bladder shape and volume can result in the bladder extending outside the GTV [15]. Onboard radiographic imaging or CBCT is used to align the patient to the treatment plan CT based on the anatomy of the pelvic bone, resulting in a 2–3 mm error [14,15,17–19]. This does not necessarily consider the relative displacement of the soft tissues (bladder) to the skeletal structure between treatments. These translational shifts in the bladder during patient setup have been measured to range up to 15 mm using CT, with a 5 mm error (SD) [15]. Similar shifts were measured using US, with errors ranging from 1 to 9 mm (SD) [20], increasing in the caudal direction. Other US image guidance methods have also been tested in prostate cancer patients, where a range of uncertainties from 1.4 to

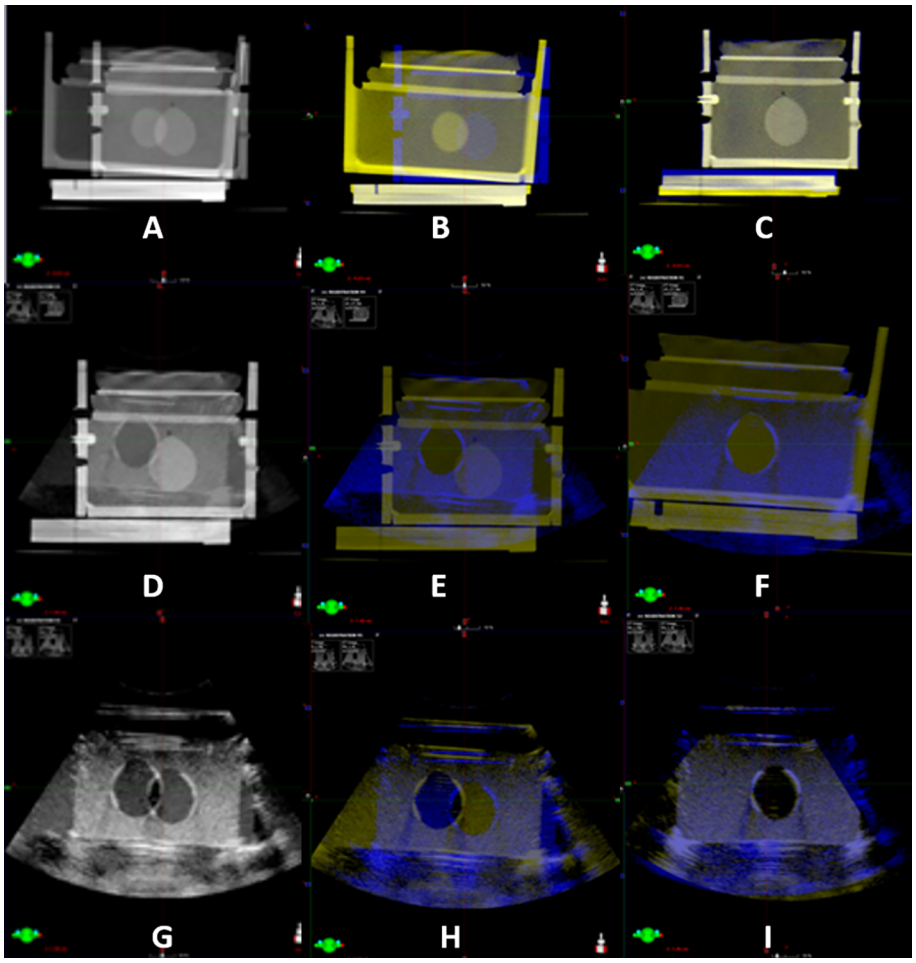

Fig. 3. Displayed are the CT-to-CT, US-to-CT, and US-to-US registration results of the bladder tissue-equivalent phantom after displacement (translation and rotation). The first column are the images prior to registration, the second column represents the displaced image in blue; the final column the images after registration. (A-C) CT-CT registration between the phantom rotated to 45° and the flat position. (D–F) US-CT registration between the phantom rotated to 45° and the flat position. (G-I) US-US registration between the phantom rotated to 45° and the flat position. (For interpretation of the references to colour in this figure legend, the reader is referred to the web version of this article.)

Table 3
Comparison of the Phantom Physical Properties to those in the Literature.

	Density (g/cm^3)		Speed of Sound (mm/μs)	
	Measured	Literature	Measured	Literature
Water	0.99	0.998 [33]	1.49	1.483 [32]
Skin	1.10	1.110–1.119 [34]	1.70	1.590–2.170 [35]
Fat	0.99	0.916 [34]	1.49	1.412–1.487 [36]
Muscle	1.06	1.038–1.056 [34]	1.59	1.589–1.603 [36]
Urine	1.03	1.001–1.050 [34]	1.55	1.554

7.9 mm (SD) have been reported [6]. A representative example, Richter et al. [21], compared the use of transperitoneal US to CBCT in patient alignment, where lateral, vertical and longitudinal uncertainties were measured to be 2.3, 2.4 and 2.7 mm (SD), respectively, with a mean Euclidean error of 3.1 mm (SD) and an overall mean discrepancy of 6 mm. In this study, the US-based platform was able to align the bladder (target) within the phantom independent of the surrounding skeletal structure. US-to-CT registration based on volumetric soft tissue contrast corrected for target (bladder phantom) misalignment and resulted in an uncertainty < 2 mm (SD), −0.4 ± 0.8 mm, 0.1 ± 0.6 mm, and −1.9 ± 0.9 mm. A potential weakness of this study was the lack of data accounting for changes in the bladder shape. These differences were reported by Lotz et al. [20] and Meijer et al. [14] to be less significant than the setup and movement errors, e.g., 1–3.5 mm (SD) and 1–3.0 mm (SD), respectively. Incorporating these errors in quadrature with the US-based platform uncertainties would result in an uncertainty (3.6 mm; SD) comparable to previous studies (3.0–5.0 mm) [14,15,17–19].

Intra-fractional motion is primarily due to bladder filling or emptying, and to a lesser degree, due to the surrounding tissue (e.g., bowel) shifting or distorting the bladder [20,22–24]. Bladder filling rates vary significantly among patients and in many cases are sufficient to cause the bladder volume to increase and extend beyond the GTV of the RT treatment plan [22]. Bladder displacements of 5–6 cm have been observed [23], with greater expansion in the superior-anterior direction [24,25]. During rectal filling, the shape of the bladder does not change much but instead shifts the volumetric center of the bladder (in SA direction). Thus, changes in the bladder volume or translation of the bladder can be used to monitor bladder filling or emptying rates [20,22]. The average shift in the bladder centroid, in the superior-anterior direction, has been measured using CBCT to be on the order of 12.0–12.5 mm over a treatment fraction [25]. This is significantly less than the statistical errors obtained when using the US-based platform, where baseline-US to US registrations were < 2.0 mm (SD) for x, y, and z translational components, and < 1.1° for rotational components, under various phantom orientations, thus providing enough precision to track bladder displacement as it is filling or emptying.

In addition to motion, ultrasound image artifacts and aberrations can also contribute to the uncertainty in patient alignment and bladder location. Two important factors that introduce image distortions include variations in the speed of sound (SOS) and acoustic refraction. US images are formed assuming a constant SOS for tissue (1.54 mm/μs); however, this does not account for the heterogenous acoustic properties within a patient, or the tissue equivalent phantoms. The resulting acoustic aberrations from this lack of homogeneity influences the positional accuracy of the bladder centroid and its shape, where different tissue types and geometries introduce axial (SOS) and lateral (refraction) displacements of the organs. In the canine tissue-equivalent

bladder phantom, the maximum axial displacement due to the skin, muscle, and bladder was calculated to shift the proximal and distal bladder wall by −0.8 and −1.3 mm, respectively. This effect can be seen in Fig. 2, the bending of the agar-plexiglass boundary at the bottom of the phantom. Similar calculations, assuming a spherical bladder, determine axial and lateral displacements of the bladder centroid and the average of the residuals in the bladder wall to be 2.5 mm and 1.3 mm respectively. Even though these systematic effects are relatively small compared to inter- and intra-fraction motion, they are not negligible. One method to reduce this uncertainty is to implement a different SOS. Changing the SOS from 1.54 to 1.52 mm/μs reduced the centroid and average wall displacements to 0.9 and 0.8 mm, respectively. However, systematic errors also dependent on the location and geometry of the transducer array, such as translational offsets of the central projection axis of the TA relative to the center of the bladder and the angle relative to the skin surface. A more robust solution would correct for the SOS variations in a patient by applying imaging processing techniques [26]. Refractive aberrations can be reduced by implementing advanced US acquisition methods [27,28], such as multi-angle or spatial compounding. These techniques have been shown to reduce angle-dependent (refractive) artifacts, such as sidelobe, shadowing, refraction and reverberation [27].

To operate the US-based platform, a coupling agent, in this case water, was used, to eliminate the need for the transducer array to be in contact with the patient. This potentially avoids displacing or distorting the tissue (up to 5–10 mm) [26], such as the bladder, due to the applied pressure from the operator. Positional flexibility was incorporated to allow the skill of the operator to maintain good US image quality without interfering with radiation treatment. This does require additional operator overhead and time, but with experience can be kept minimal. Another weakness was the inability to automatically register US to CT without user involvement. Development of advanced registration algorithms will be necessary. This design of the US-based platform also made a conscious effort to consider future use of complementary ultrasound-based functionality (photoacoustics, radioacoustics, Doppler) to monitor functional and molecular properties of tissue, specifically blood flow [29] and hypoxia [30], and in-vivo dosimetry for applications in other therapeutic techniques, such as hyperthermia, anti-angiogenesis and particle therapy [31].

An ultrasound-based platform was designed and calibrated to provide a low-cost hands-fee device for image-guidance in radiation treatment of canine bladder cancer patients. To evaluate the applicability of this device, a CT/US tissue-equivalent phantom was fabricated and used to realign the bladder to the CT treatment plan using 3D US and to a baseline 3D US image with a statistical uncertainty < 2 mm, if couch repositioning was within 5 degrees of rotation. This uncertainty is consistent with current radiological techniques used in patient alignment (inter-fraction) and sufficient to monitor intra-fractional changes in the bladder. Future work will evaluate how to utilize these techniques and adapt RT in canine bladder patients and potentially human patients.

Source of financial support/funding statement:

The authors have no relevant sources of financial support/funding to disclose.

Declaration of Competing Interest

The authors declare that they have no known competing financial interests or personal relationships that could have appeared to influence the work reported in this paper.

Appendix A. Supplementary data

Supplementary data to this article can be found online at https://doi.org/10.1016/j.phro.2019.10.003.

References

[1] Sommer BC, Dhawan D, Ratliff TL, Knapp DW. Naturally-occurring canine invasive urothelial carcinoma: a model for emerging therapies. Bladder Cancer 2018;4:149–59.
[2] Poirier VJ, Forrest LJ, Adams WM, Vail DM. Piroxicam, mitoxantrone, and coarse rraction radiotherapy for the treatment of transitional cell =carcinoma of the bladder in 10 dogs: a pilot study. J Am Aim Hosp Assoc 2004;40:131–6.
[3] Marconato L, Nitzl DB, Melzer-Ruess KJ, Keller MA, Buchholz J. Chemotherapy and radiation therapy in 4 dogs with muscle-invasive transitional cell carcinoma of the urinary tract. Can Vet J 2012;53:875–9.
[4] Muren LP, Smaaland R, Dahl O. Organ motion, set-up variation and treatment margins in radical radiotherapy of urinary bladder cancer. Radiother Oncol 2003;69:291–304.
[5] Zhang S, Yu Y-H, Zhang Y, Qu W, Li J. Radiotherapy in muscle-invasive bladder cancer: the latest research progress and clinical application. Am J Cancer Res 2015;5:854–68.
[6] Muren LP, Redpath AT, Lord H, McLaren D. Image-guided radiotherapy of bladder cancer: bladder volume variation and its relation to margins. Radiother Oncol 2007;84:307–13.
[7] Fontanarosa DS, van Der Meer J, Bamber E, Harris T, O'SheaVerhaegen F. Review of ultrasound image guidance in external beam radiotherapy: I. Treatment planning and inter-fraction motion management. Phys Med Biol 2015;60:R77–114.
[8] O'Shea T, Bamber J, Fontanarosa D, van Der Meer S, Verhaegen F, Harris E. Review of ultrasound image guidance in external beam radiotherapy: II. Intra-fraction motion management and novel applications. Phys Med Biol 2016;61:R90–137.
[9] Murphy MJ, Balter J, Balter S, BenComo JA, Das IJ, Jiang SB, et al. The management of imaging dose during image-guidedradiotherapy: report of the AAPM Task Group 75. Med Phys 2007;34:4041–63.
[10] Sen HT, Bell MAL, Iordachita I, Wong J, Kazanzides P. A cooperatively controlled robot for ultrasound monitoring of radiation therapy. Rep US 2013:3071–6.
[11] Chadha M, Young A, Geraghty C, Masino R, Harrison L. Image guidance using 3D-ultrasound (3D-US) for daily positioning of lumpectomy cavity for boost irradiation. Radiat Oncol 2011;6:45.
[12] Fraser DJ, Chen Y, Poon E, Cury FL, Falco T, Verhaegen F. Dosimetric consequences of misalignment and realignment in prostate 3DCRT using intramodality ultrasound image guidance. Med Phys 2010;37:2787–95.
[13] Klein EE, Hanley J, Bayouth J, Yin F-F, Simon W, Dresser S, et al. Task Group 142 report: quality assurance of medical accelerators. Med Phys 2009;36:4197–212.
[14] Meijer GJ, Rasch C, Remeijer P, Lebesque J. Three-dimensional analysis of delineation errors, setup errors, and organ motion during radiotherapy of bladder cancer. Int J Radiat Oncol Biol Phys 2003;55:1277–87.
[15] Redpath AT, Muren LP. CT-guided intensity-modulated radiotherapy for bladder cancer: isocentre shifts, margins and their impact on target dose. Radiother Oncol 2006;81:276–83.
[16] Knapp DW, Ramos-Vara JA, Moore GE, Dhawan D, Bonney PL, Young KE. Urinary bladder cancer in dogs, a naturally occurring model for cancer biology and drug development. ILAR J 2014;55(1):100–18.
[17] O'Shea TP, Garcia LJ, Rosser KE, Harris EJ, Evans PM, Bamber JC. 4D ultrasound speckle tracking of intra-fraction prostate motion: a phantom-based comparison with x-ray fiducial tracking using CyberKnife. Phys Med Biol 2014;59:1701–20.
[18] Abramowitz MC, Bossart E, Martin L, Brooks R, Lathuiliere F, Laura F, et al. Noninvasive real-time prostate tracking using a transperineal ultrasound: a clinical trial comparison to rf transponders with visual confirmation. Int J Radiat Oncol Biol Phys 2013;87:S682.
[19] Feigenberg SJ, Paskalev K, McNeeley S, Horwitz EM, Konski A, Wang L, et al. Comparing computed tomography localization with daily ultrasound during image-guided radiation therapy for the treatment of prostate cancer: a prospective evaluation. J Appl Clin Med Phys 2007;8:99–110.
[20] Lotz HT, Remeijer P, van Herk M, Joos V, deBois JA, Zijp LJ, et al. A model to predict bladder shapes from changes in bladder and rectal filling. Med Phys 2004;31:1415–23.
[21] Richter A, Polat B, Lawrenz I, Weick S, Sauer O, Flentje M, et al. Initial results for patient setup verification using transperineal ultrasound and cone beam CT in external beam radiation therapy of prostate cancer. Radiat Oncol 2016;11:147-.
[22] McBain CA, Green MM, Stratford J, Davies J, McCarth C, Taylor B, et al. Ultrasound imaging to assess inter- and intra-fraction motion during bladder radiotherapy and its potential as a verification tool. Clin Oncol (R Coll Radiol) 2009;21:385–93.
[23] McBain CA, Khoo VS, Buckley DL, Sykes JS, Green MM, Cowan RA, et al. Assessment of bladder motion for clinical radiotherapy practice using cine-magnetic resonance imaging. Int J Radiat Oncol Biol Phys 2009;75:664–71.
[24] Dees-Ribbers HM, Betgen A, Pos FJ, Witteveen T, Remeijer P, van Herk M. Inter- and intra-fractional bladder motion during radiotherapy for bladder cancer: a comparison of full and empty bladders. Radiother Oncol 2014;113:254–9.
[25] Foroudi F, Pham D, Bressel M, Gill S, Kron T. Intrafraction bladder motion in radiation therapy estimated from pretreatment and posttreatment volumetric imaging. Int J Radiat Oncol Biol Phys 2013;86:77–82.
[26] Fontanarosa D, van der Meer S, Harris E, Verhaegen F. A CT based correction method for speed of sound aberration for ultrasound based image guided radiotherapy. Med Phys 2011;38:2665–73.
[27] Heng HG, Widmer WR. Appearance of common ultrasound artifacts in conventional vs. spatial compound imaging. Vet Radiol Ultrasound 2010;51:621–7.
[28] Jespersen SK, Wilhjelm JE, Sillesen H. Multi-angle compound imaging. Ultrason Imaging 1998;20:81–102.
[29] Pilatou MC, Marani E. de Mul FFM, and Steenbergen. Photoacoustic imaging of

brain perfusion on albino rats by using evans blue as contrast agent. Arch PhysiolBiochem 2003;111:389–97.
[30] Heiss WD, Raab P, Lanfermann H. Multimodality assessment of brain tumors and tumor recurrence. J Nucl Med 2011;52:1585–600.
[31] Alsanea F, Moskvin V, Stantz KM. Feasibility of RACT for 3D dose measurement and range verification in a water phantom. Med Phys 2015;42:937–46.
[32] Greenspan M, Tschiegg CE. Tables of the Speed of Sound in Water. J Acoust Soc Am 1959;31:75–6.
[33] Jones FE, Harris GL. ITS-90 Density of water formulation for volumetric standards and calibration. J Res Nat Inst Stand Technol 1992;97:335–40.
[34] Woodard HQ, White DR. The composition of body tissues. Br J Radiol 1986;59:1209–18.
[35] O'Brien WD, Olerud J, Shung KK, Reid JM. Quantitative acoustical assessment of wound maturation with acoustic microscopy. J Acoust Soc Am 1981;69:575–9.
[36] Nasoni RL, Bowen T, Conner WG, Sholes RR. In vivo temperature dependence of ultrasound speed in tissue and its applications to noninvasive temperature monitoring. Ultrason Imaging 1979;1:34–43.